

The Effect of HVOF Spray Distance on Solid Particle Erosion Resistance of WC-Based Cermets Bonded by Co, Co-Cr and Ni Deposited on Mg-Alloy Substrate

Ewa Jonda^{1*}, Leszek Łatka², Aleksandra Lont³, Klaudiusz Gołombek⁴, Mirosław Szala⁵

¹ Department of Engineering Materials and Biomaterials, Silesian University of Technology, ul. Konarskiego 18a., 44100 Gliwice, Poland

² Department of Metal Forming, Welding and Metrology, Faculty of Mechanical Engineering, Wrocław University of Science and Technology, ul. Łukasiewicza 5., 50371 Wrocław, Poland

³ Welding Department, Faculty of Mechanical Engineering, Silesian University of Technology, ul. Konarskiego 18a., 44100 Gliwice, Poland

⁴ Materials Research Laboratory, Silesian University of Technology, ul. Konarskiego 18a., 44100 Gliwice, Poland

⁵ Department of Materials Engineering, Faculty of Mechanical Engineering, Lublin University of Technology, ul. Nadbystrzycka 36., 20618 Lublin, Poland

* Corresponding author's e-mail: ewa.jonda@polsl.pl

ABSTRACT

Magnesium alloys are very interesting engineering materials because of their high strength-to-density ratio. On the other hand, they are characterized by low hardness as well as low erosion resistance. Because of these reasons, their applications in the industry are very limited. The article presents the results of the high velocity oxy-fuel (HVOF) spraying of the hard cermet coatings onto AZ31 magnesium alloy substrate. Three feedstock powders were used in the process with composition (wt.%): WC-12Co, WC-10Co-4Cr and WC-20Cr₃C₂Ni. The spray distance (SD) was selected as a variable parameter with values equal to 320 and 400 mm. Observations carried out under a scanning electron microscope (SEM) revealed a typical HVOF-sprayed microstructure with a compact structure and low porosity (below 3 vol.%). The hardness of the manufactured coatings, ranging from 912 HV0.2 to 1328 HV0.2, what was significantly higher than the substrate. The solid particle erosion tests were carried out according to the ASTM G76-04 standard. Erosive experiments were done for 30°, 60° and 90° inclination angles of the nozzle using Al₂O₃ abrasive. Erosion tests confirm that cermets exhibit substantial erosion resistance better than the substrate. The highest erosion resistance was noted for WC-10Co-4Cr coatings. The erosion rate for cermet coatings was mostly below 0.9 mg/min, whereas for the AZ31 it was more than 1.5 mg/min. In the case of the average erosion value, it was between 12 and 22 times lower than for the substrate. Results analysis reveal that shorter spray distance decreases porosity, increases hardness, and finally supports erosion resistance of the cermets.

Keywords: HVOF spraying, thermal spraying, erosion, cermet, coatings, AZ31, solid particle erosion, microstructure.

INTRODUCTION

Current expectations in the industry are related to constantly growing requirements regarding device parameters, extended operating time and cheaper service. Such multi-dimensional expectations are not easily achievable, especially in a situation of shrinking natural resources and rising

prices at the same time. Therefore, we can increasingly observe situations in which, instead of focusing on inventing new materials, scientists and engineers try to improve existing ones. Research on magnesium alloys fits into these trends [1–3]. The most important advantages of such material are low density and, consequently low value of the specific strength [4]. On the other hand, there are

crucial drawbacks which defects that prevent the wide use of these materials, e.g. low hardness, poor corrosion-, wear- and erosion resistance [5,6].

In order to improve the surface of the magnesium alloys, the two routes are possible. The first option is surface modification. It could be done by many methods, however part of them is not suitable for magnesium alloys. The valuable review of this area was given by Morelli et al. [7]. The second way is connected with coatings deposition using thermal spray methods. In such case there are some limitations connected with the flammability of the magnesium alloys [8] and high plasticity [9] from the one hand. On the other hand, there are some limitations according to the methods and feedstock materials, e.g., in case of the cermet coatings deposition. Among many thermal spray methods, the high velocity oxy-fuel (HVOF) is characterized by homogenous structure with low porosity level, as well as low crack density [10–12]. It is caused by relatively low flame temperature and high particles velocity [13–15] in comparison to atmospheric plasma (APS) and suspension plasma spraying (SPS) [16,17].

In the available literature on the discussed issue, the aspect related to the difficulty in selecting the parameters of the process of spraying cermet coatings on a relatively soft substrate material, especially aluminum alloys is repeatedly described [18–21]. Usually structural stainless steel or nickel alloys are commonly used as substrate materials [12,22,23]. These alloys show relatively high melting points, which facilitates the selection of HVOF process parameters to obtain high-quality coating and prevent melting down the substrate. In the case of aluminum or magnesium alloy substrate, the deposition of high-quality cermet coatings seems a tricky task that must solve the problem to achieving sufficient spraying temperature (to liquidate the cermet feedstock cobalt or nickel-based matrix) and maintaining the temperature of the substrate below its melting point. This makes the appropriate selection of deposition parameters on magnesium substrate challenging, especially in the case of Co-WC and Ni-WC based cermets manufactured on AZ31 magnesium alloy. Successful selection of the technological spraying parameters was shown in the current research.

HVOF coatings deposited on magnesium alloy substrates could be a promising solution in the automotive and aerospace industries because they allow for mass reduction. Some works in the literature were made in the field of

corrosion resistance of cermet coatings [22,24]. Nevertheless, a literature gap exists in cermet coatings manufactured on magnesium alloys and their deep investigations to verify the operational properties of cermets deposited using specific technological parameters. One such way is a solid particle erosion resistance. The second issue is the selection of the key HVOF process parameters and their impact on microstructure and such properties. One of the most important parameters is spray distance, especially in industrial conditions, which is relatively easy to change [25]. As mentioned before, the appropriate selection of spray distance guarantees the high quality of the deposited coatings and prevents the magnesium substrate from melting, which was revealed in the current study. This research results are part of a broad experimental plan regarding the properties of coatings thermally sprayed using the HVOF method on light material substrates such as magnesium alloys of the AZ31 series. The work is a continuation of research aimed at determining the impact of the applied process parameters on the functional properties of the applied coatings. In our previous work, corrosion resistance, abrasive wear and cavitation erosion were tested [26,27]. Moreover, the detailed microstructure investigations were carried out [28]. Testing the resistance of coatings to erosive wear caused by solid particles is the next stage of the research plan.

Current investigations aimed to assess the influence of microstructure, hardness, and surface morphology on solid particle erosion resistance of cermet coatings: WC-12Co, WC-10Co-4Cr and WC-20Cr₃C₂-7Ni manufactured by HVOF on AZ31 magnesium alloy substrate using different spraying distance equal to 320 mm and 400 mm. Additionally, the mechanisms of erosion wear of deposited coatings were identified. This paper fills the literature gap in state of the art on cermet coatings deposited on the light materials substrate. Also it provides the original comparison of erosive resistance of a set of different nickel and cobalt-based binder cement systems sprayed on AZ31 substrate.

MATERIALS AND METHODS

In current studies three commercially available cermet powders: (i) WC-12wt.%Co (Amperit 558.074, Höganäs), (ii) WC-10wt.%Co-4wt.%Cr (Amperit 518.074, Höganäs) and (iii) WC-20wt.%Cr₃C₂-7wt.%Ni (Woka 3702-1, Oerlikon

Metco) were used as feedstock in the deposition process. For all powders the delivery conditions were the same, agglomerated and sintered. The feedstock powders morphologies are presented on Figure 1. For all powder types the delivery state was agglomerated and sintered. Moreover, the particles exhibit spherical shape which is preferential from the its flowability point of view.

The particle size distribution declared by the manufacturer ($-45 + 15 \mu\text{m}$) was confirmed by own measurements (see Table 1) carried out with particle size analyzer set-up (PSA 1190, Anton Paar). The detailed analysis of the feedstock powders can be found in [26].

The substrate material used in current study was magnesium alloy AZ31. The specimens were prepared as a circle with 100 mm diameter and 5 mm thickness. Before spraying the substrates were sand blasted in order to obtain specific surface roughness (R_a about $3 \mu\text{m}$) and cleaned with ethanol. The deposition process was carried out

using a spray system JP 5000 TAFE (Indianapolis, USA) from RESURS Company (Warsaw, Poland). The constant process parameters were equal to as follow, oxygen feed rate: 900 (slpm), kerosene feed rate: 0.435 (slpm), nitrogen feed rate: 12 (slpm), powder feed rate: 70 (g/min) and water flow: 23 (slpm). The spray distance (SD) was selected as a variable parameter. Sample codes, as well as the SD value variations, are collected in Table 2.

The microstructure analysis of the manufactured coatings was carried out Scanning Electron Microscope with secondary electron and back-scattered detectors (Supra 35, Zeiss, Oberkochen, Germany) which was equipped with EDS (Energy Dispersive X-ray Spectrometer) analyzer (Supra 35, Zeiss, Oberkochen, Germany) in order to determine chemical composition. Before the tests, additional calibration of the EDS system was performed on real standards for all elements, including carbon.

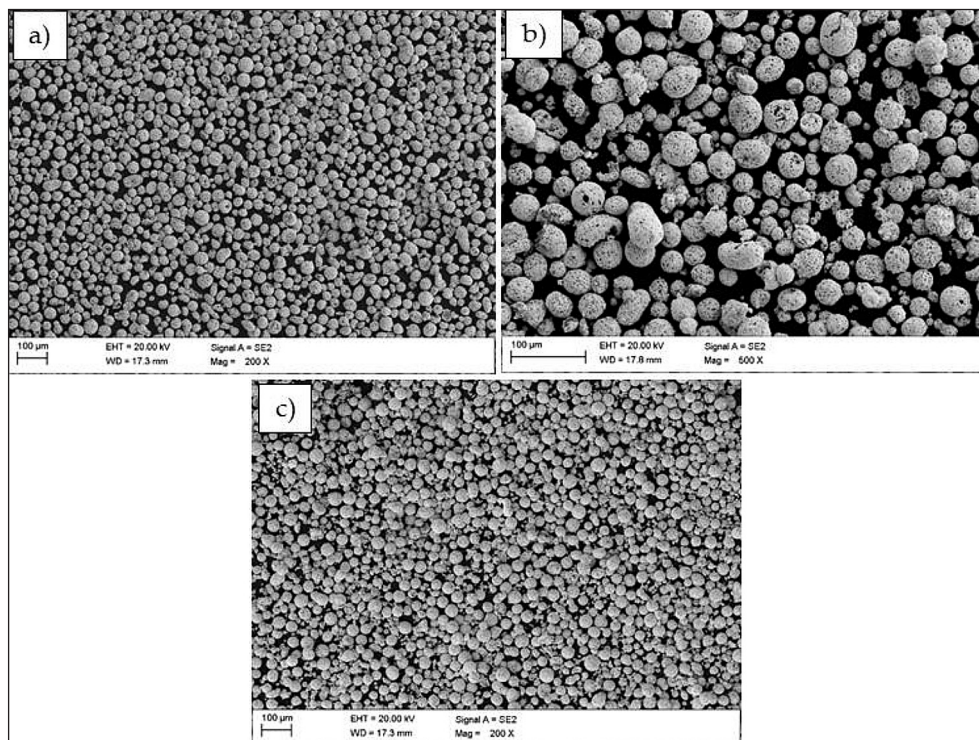


Figure 1. The feedstock powders morphologies: (a) WC-12Co (b) WC-10Co-4Cr (c) WC-20Cr₃C₂-7Ni (SEM)

Table 1. The particle size distribution of the feedstock powders used for HVOF spraying

Size distribution	WC-12Co	WC-10Co-4Cr	WC-20Cr ₃ C ₂ -7Ni
$d_{10}, \mu\text{m}$	19.92 ± 0.24	17.41 ± 0.22	17.94 ± 0.15
$d_{50}, \mu\text{m}$	35.26 ± 0.20	34.04 ± 0.14	36.33 ± 0.22
$d_{90}, \mu\text{m}$	56.54 ± 0.28	57.70 ± 0.18	61.84 ± 0.40

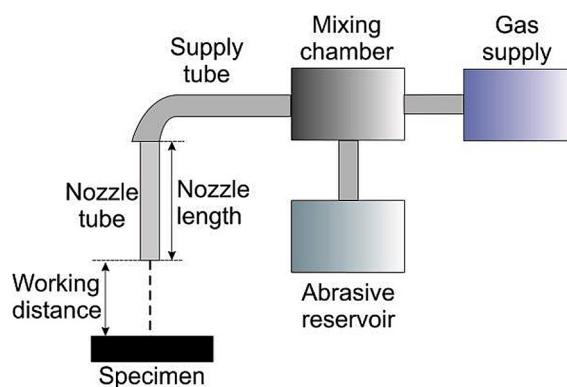
Table 2. Sample code and values of the variable HVOF process parameters

Sample code	Feedstock powder	Spray distance, mm
C1-320	WC-12Co	320
C1-400		400
C2-320	WC-10Co-4Cr	320
C2-400		400
C3-320	WC-20Cr ₃ C ₂ -7Ni	320
C3-400		400

Image analysis with free software ImageJ (version 1–50) was used to determine the porosity level. The measurements were made according to the ASTM E2109-01 standard. The porosity was assessed as an average from 20 images at 1000× magnification. Scanning Electron Microscope with secondary electron and backscattered detectors (Supra 35, Zeiss, Oberkochen, Germany) was used for topography investigations of the deposited coatings. The surface roughness of sprayed coatings was measured by a stylus profilometer (MarSurf PS 10, Mahr, Germany), according to the ISO 4288 standard, with Gaussian filters according to the ISO 16610-21 standard. Five Ra and Rz parameter measurements were performed for each sample. Then, calculate the average and standard deviation values. The Vickers hardness was estimated at the sample cross-sections under the load equal to 1.96 N (HV0.2) using the HV-1000 hardness tester (Sinowon Innovation Metrology, Dongguan, China), according to the ISO 4516 standard. For each coating, 12 indentations were made and then the average and standard deviation values were calculated.

Erosion resistance tests at room temperature were carried out on a specially designed test stand at the Welding Department of the Silesian University of Technology in Gliwice according to ASTM G76-04 standard. Figure 2 shows the schematic diagram of the erosion resistance test rig according to the ASTM G76-04 standard.

The test was performed using a nozzle tube with a diameter of 1.5 ± 0.075 mm and located 10 ± 1 mm from the sample. The inclination angles of the nozzle relative to the sample were 30°, 60° and 90°, respectively. The test uses Al₂O₃ abrasive with a particle size of 50 μm (Figure 3), the particle feed amount was 2 ± 0.5 g/min, and the nozzle exit speed was 70 m/s. The test duration was 10 minutes, all tests carried out in the as-sprayed state. To obtain reliable results, 10 tests were performed using the given parameters. The

**Figure 2.** Scheme of solid particle erosion equipment (according to the ASTM G76)

quantitative result of these tests was the mass loss using a laboratory scale with 0.1 mg accuracy. According to the ASTM G76-04 standard, the erosion rate and the erosion value were calculated. Moreover, the SEM observations were carried out in order to determine the wear mechanism.

RESULTS AND DISCUSSION

All coatings were deposited in order to achieve a thickness c.a. 250 μm. As expected, the coatings exhibit a dense and homogenous structure. Moreover, the good filling of the substrate surface irregularities could be seen (Fig. 4). It is a result of the specific conditions, especially high velocity of the molten powder particles, which is characteristic for the HVOF method. Similar structure could be found in [29,30].

The detailed observations at higher magnification (Fig. 5) confirmed the fine structure of the all coatings. The tungsten and chromium carbides are uniformly distributed in the hole samples volume. On the other hand, both metallic matrixes were melted and correct wetted hard particles. Some imperfections could be observed, as cracks, pores and voids. It is probably a result

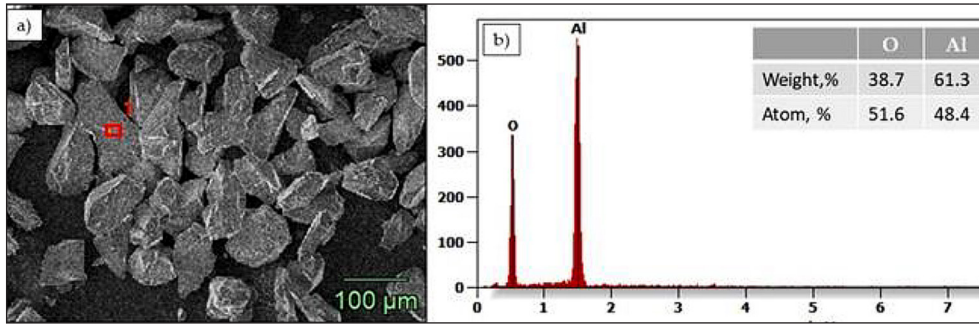


Figure 3. (a) the morphology of the Al_2O_3 abrasive (SEM) used in erosive tests and the (b) results of chemical analysis (SEM-EDS)

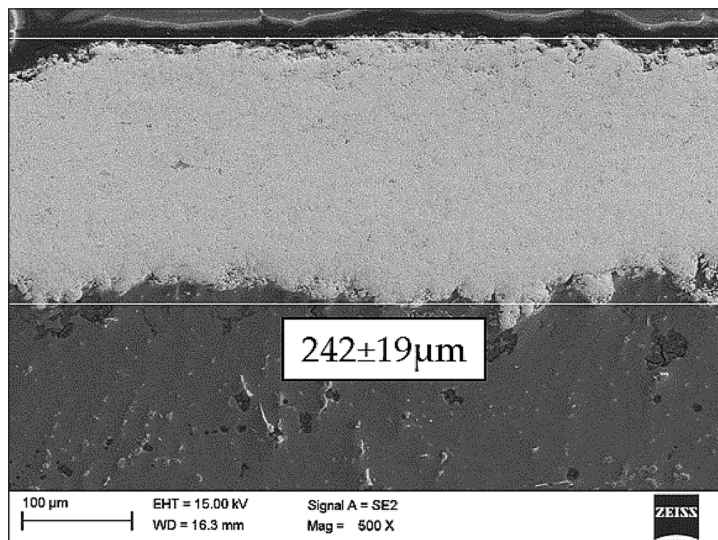


Figure 4. SEM image of the C2-320 samples cross-section

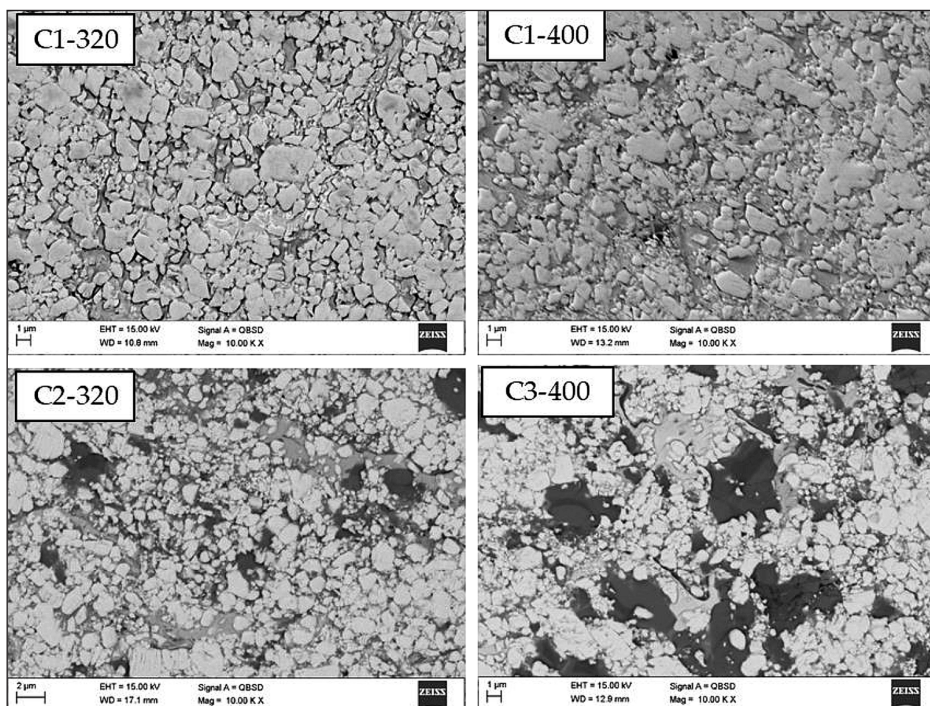


Figure 5. The microstructure of the manufactured samples (SEM)

of the thermal stresses caused by the deposition process [31] as well as short time in which the particles stay in the relative low-temperature flame (c.a. 3200 K) [32,33]. The analysis of chemical composition were carried out on the polished cross-sections of tested coatings, in the points marked in Figure 6, in order to confirm the presence of elements. The EDS results are collected in Table 3 and were calculated using the ZAF correction.

The porosity values of the manufactured coatings were at the level for typical HVOF deposits. Even for samples sprayed from 400 mm, the porosity was relatively low (below 3 vol.%). Detailed results are collected in Table 4. Similar results could be found in [34–36]. Two reasons may cause the differences in the porosity values for investigated coatings. First is a type of matrix material. Nickel is a slightly softer metal than cobalt and has a lower melting point [37]. On the other hand, longer spray distance (SD) makes it impossible to obtain a compact structure because of reduced particles velocity [38]. In Table 4, the influence of the spray distance on the coatings' porosity value is clearly visible, which was also reported by Murugan et al. [39].

The hardness of the manufactured coatings is presented in Figure 7. It could be seen that reducing the spray distance plays an important role in improving hardness. It is a result of more compact structure as well as reduced porosity [40,41]. Similar hardness values to those in current studies could be found in [42, 43]. The surface of the obtained coatings is rather smooth for standoff distance (SD) equal to 320 mm (Fig. 8 left column). At some areas, minor irregularities could be observed. In case of SD equal to 400 mm (Fig. 8 right column) there are some craters which caused increasing surface roughness. Nevertheless, for all manufactured coatings their topography is typical

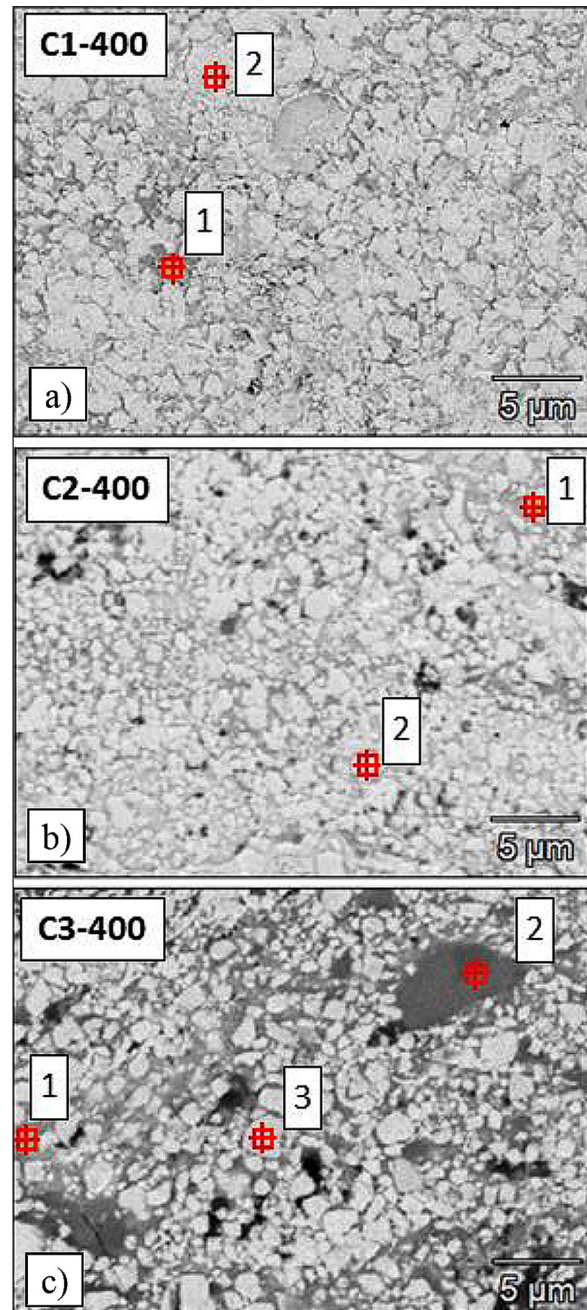


Figure 6. The detailed microstructure of the manufactured samples (SEM) with EDS points: (a) C1-400 (b) C2-400, C3-400

Table 3. EDS results of the investigated coatings (spots marked in Fig. 6), SEM

Sample code	C1-400				C2-400				C3-400					
	Point 1		Point 2		Point 1		Point 2		Point 1		Point 2		Point 3	
Point	wt.%	at.%												
W	58.3	29.1	96.5	66.2	52.2	20.9	96.7	66.6	47.2	16.9	14.9	3.8	96.4	63.9
C	1.0	7.7	3.5	33.8	2.6	16.1	3.3	33.4	4.2	23.2	6.4	25.0	3.6	36.1
Co	40.7	63.2	–	–	28.1	35.2	–	–	–	–	–	–	–	–
Cr	–	–	–	–	17.1	27.8	–	–	34.2	43.6	77.9	70.5	–	–
Ni	–	–	–	–	–	–	–	–	14.4	16.3	0.9	0.7	–	–

Table 4. Average values of porosity for the manufactured coatings (in vol.%)

C1-320	C1-400	C2-320	C2-400	C3-320	C3-400
1.9 ± 0.5	2.7 ± 0.6	2.3 ± 0.5	3.0 ± 0.6	1.3 ± 0.4	2.0 ± 0.5

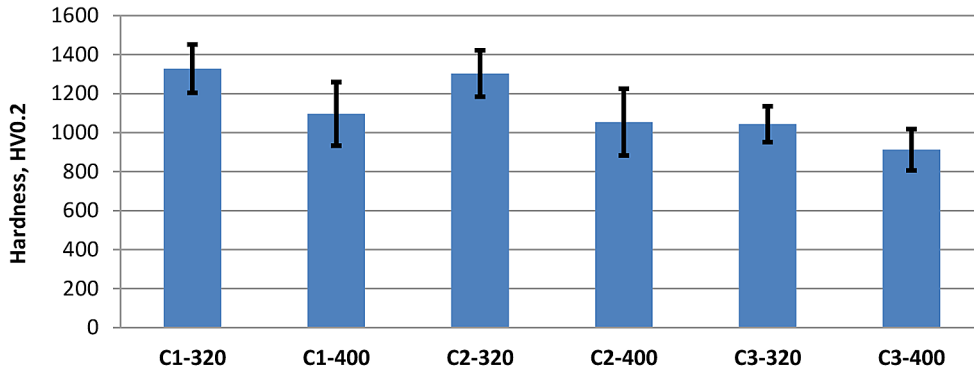


Figure 7. The average hardness values of the deposited coatings

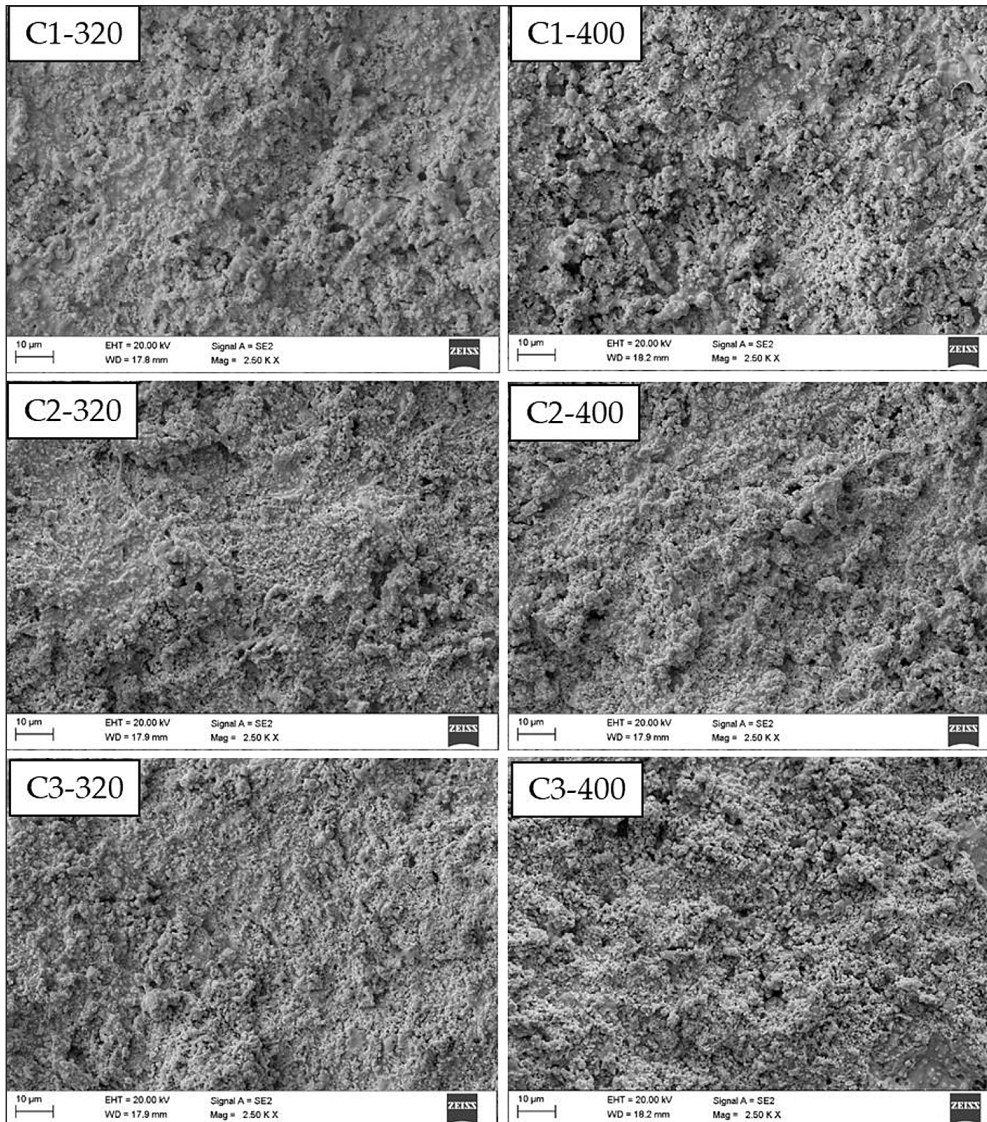


Figure 8. The surface topography of the manufactured HVOF cermet coatings (SEM)

for HVOF deposits [44,45]. The observed irregularities are connected with carbide particles that exhibit high melting points and remain solid during flight in the flame [46]. The surface roughness of the as-sprayed coatings is presented in Table 5. These values are relatively close to the literature data [34,47]. The coatings with cobalt matrix show a slight decrease in roughness with the increasing SD. It could be caused by decreasing particles velocity and, consequently, kinetic energy [48]. It results in smaller surface deformations. In general, the surface roughness values (for both factors) differ slightly in the standard deviation range. Therefore, there was no clear relationship between the spray parameters, feedstock material type and the surface morphology of coatings.

The results of the solid particle erosion tests are presented in Figure 9. It is clearly observed that HVOF coatings strongly improved the erosion resistance in comparison to the substrate material. As can be seen, the average erosion rate (AER) for all coatings is around double, sometimes even 2.5 times, lower than for AZ31. Moreover, the results confirmed that for bulk metal alloys, the most dangerous impact angle is 30°, whereas for ceramic materials, it is 90° [49]. In case of the cermet materials, the maximum erosion rate is connected with the impact angle c.a. 60° [50]. Analysing Figure 9, it can be seen that for all impact angles, as well as all

coating materials, the lower SD results in better erosion resistance. Among tested samples, the best performance exhibits C2-320. The excellent erosion resistance is characteristic in the case of WC-10Co-4Cr coatings [51,52]. The novelty of current investigation is confirmation assumed hypothesis that changing substrate material onto the light Mg-based alloy with correct process parameters makes possible obtaining coatings without deterioration of its properties. In Figure 10 were presented the results of the average erosion value (AEV). It is calculated as material volume loss in relation to the total mass of erodent. In this case, the impact angle equal to 60° was also the most hazardous for the cermet coatings. Moreover, the differences between coatings and AZ31 substrate are much and more significant than for AER due to almost seven times higher density of cermet materials than the magnesium alloy. For better readability of AEV values for cermet coatings, its results were presented in separate plot (Fig. 11).

Erosive results and surface morphology and analysis indicate a negligible effect of surface roughness (Tab. 5) of as-sprayed coatings on the erosion rate (Fig. 9). On the other hand, research confirms that the hardness and uniformity of the coatings have a crucial effect on the erosion resistance of the coatings. It can be deduced from Table 4 and Figure 7 that a shorter spray distance i.e. 320 mm, decreases the porosity and increases

Table 5. The average roughness value (Ra and Rz) of the manufactured coatings

Roughness parameter	C1-320	C1-400	C2-320	C2-400	C3-320	C3-400
Ra, μm	3.81 ± 0.27	3.59 ± 0.24	4.08 ± 0.24	3.82 ± 0.17	4.55 ± 0.44	4.60 ± 0.34
Rz, μm	22.25 ± 1.86	20.98 ± 1.08	23.30 ± 0.87	22.60 ± 1.50	25.14 ± 2.17	27.92 ± 1.84

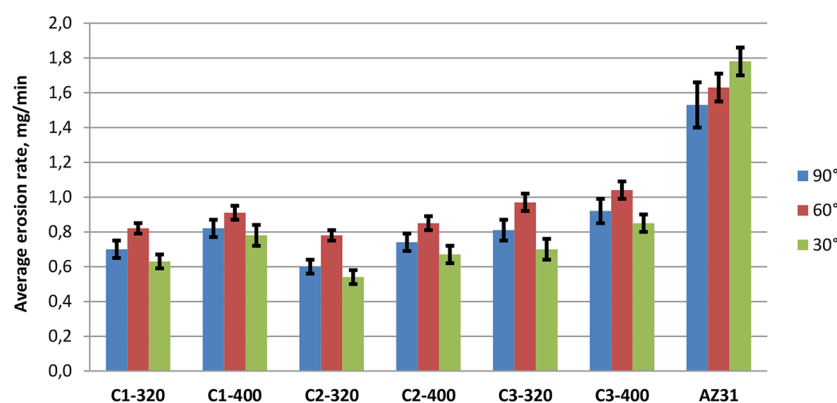


Figure 9. The average erosion rate of the sprayed cermet coatings and the AZ31 substrate

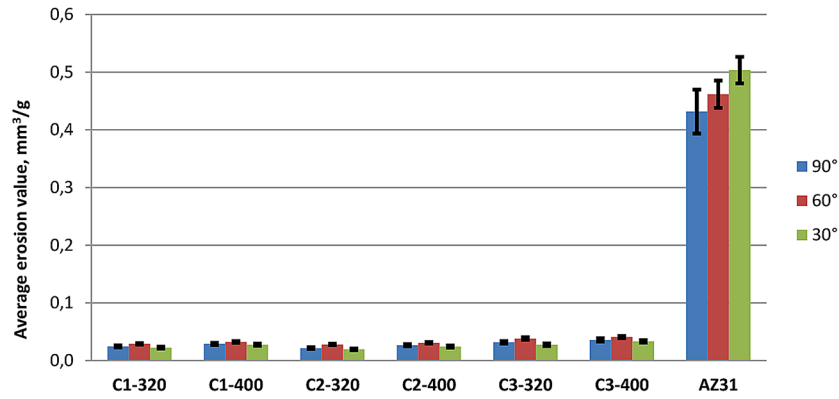


Figure 10. The average erosion value of the sprayed cermet coatings and the AZ31 substrate

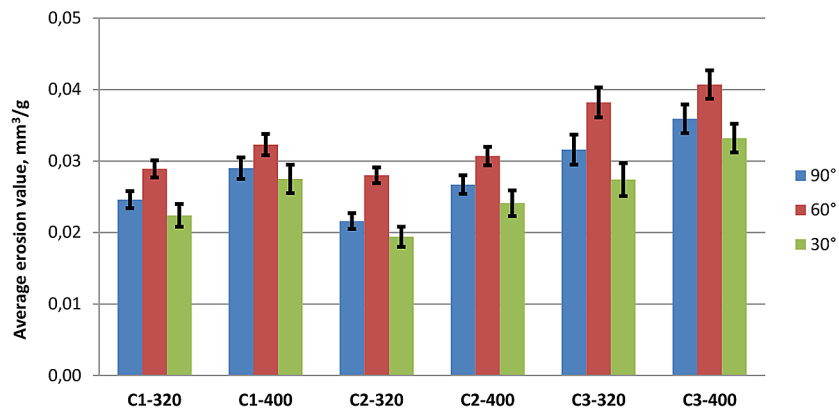


Figure 11. The average erosion value of the sprayed cermet coatings

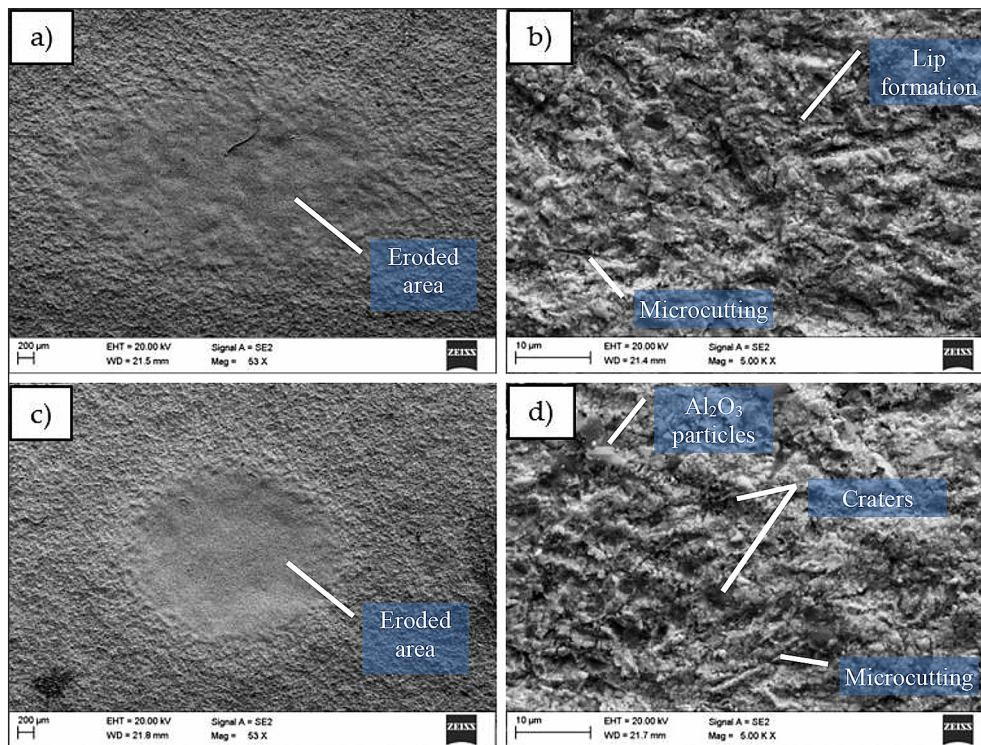


Figure 12. The SEM micrographs of erosive craters for C3-320 (left column: general view, right column: detailed view): (a),(b) impact angle 30°; (c),(d) impact angle 60°; (e),(f) impact angle 90°

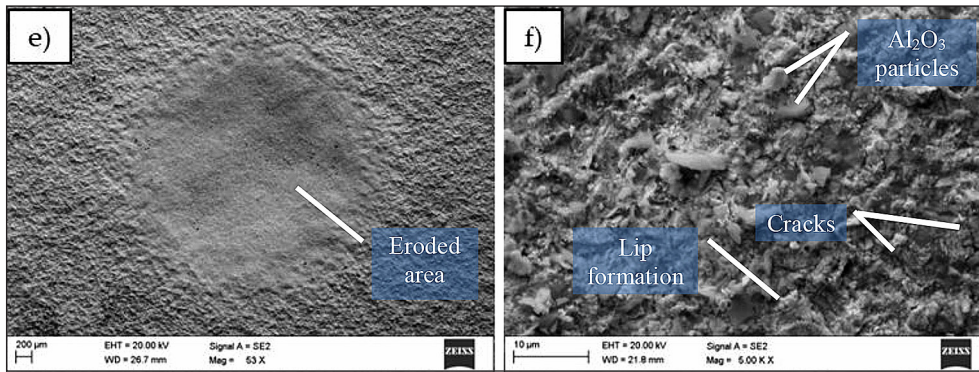


Figure 12. Cont. The SEM micrographs of erosive craters for C3-320 (left column: general view, right column: detailed view): (e),(f) impact angle 90°

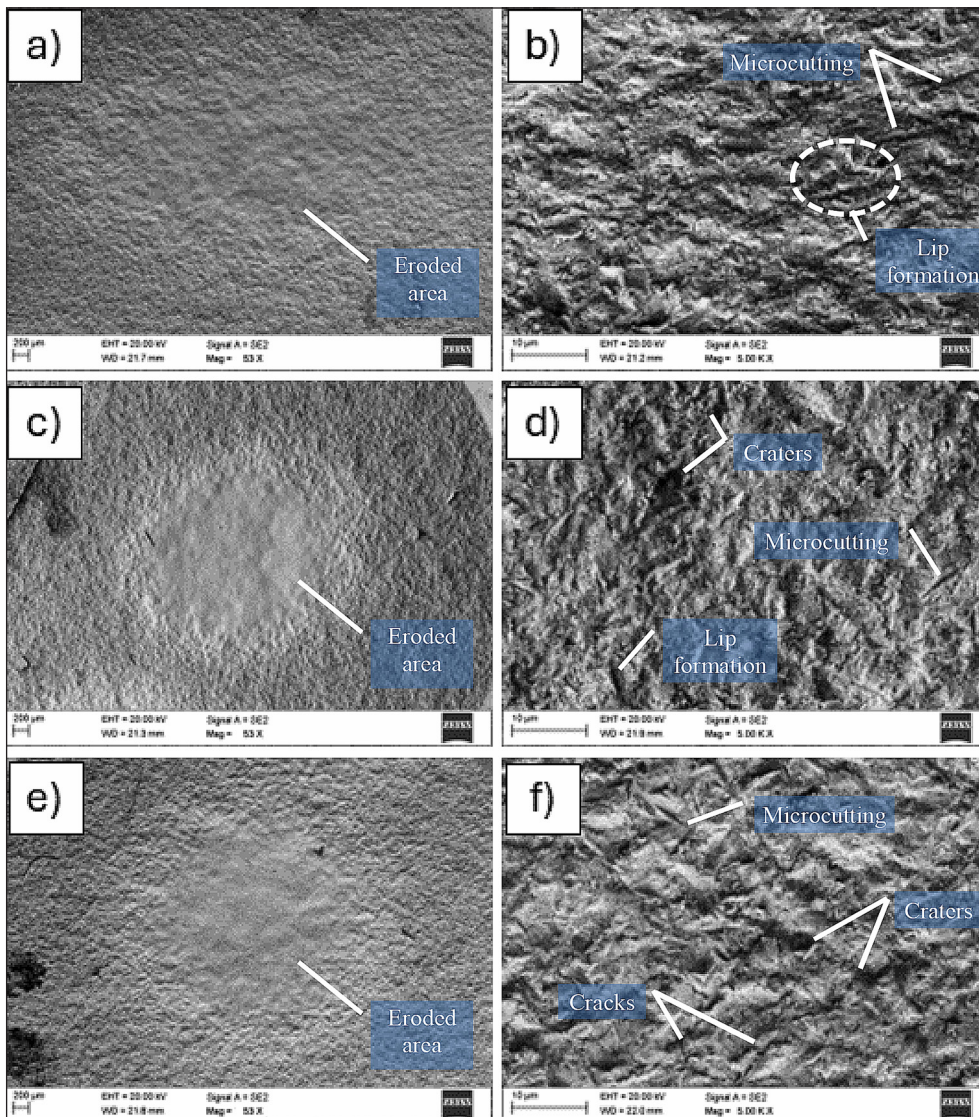


Figure 13. The SEM micrographs of erosive craters for C2-320 (left column: general view, right column: detailed view): (a),(b) impact angle 30°; (c),(d) impact angle 60°; (e),(f) impact angle 90°

each coating's hardness. Combining the hardness (Fig. 7) with erosion results (Fig. 9; Fig. 10) confirms that coatings sprayed from 320 mm standoff

distance are harder and show a lower material loss rate than those deposited with 400 mm distance. The exemplary eroded craters, due to solid

erosion particle tests at different impact angles, were compared in Figure 12 (for C3-320) and Figure 13 (for C2-320). At an angle equal to 30°, the main erosion process is associated with microcutting and grooving (lip formation) of the coating material (Fig. 12b; Fig. 13b). During the test, the carbide particles are exposed because of the matrix removal. It results in the displacement and, finally detachment of these particles, especially under the small impact angle. Similar behaviour was observed by Gonzalez et al. [50]. In case of impact angles equal to 60° and 90°, the erosion mechanism was changed. The main reason for the material loss is the formation of the craters. This behaviour is characteristic for brittle materials [53]. Nevertheless, the most eroded surface, with many pits, empty areas after carbide removal due to fatigue action of erodent, microcutting and cracks are visible, which is a characteristic feature for an impact angle equal to 60° (Fig. 12c,d and Fig. 13c,d). Lip formation and brittle behaviour result from the mixed nature of cermet, consisting of metallic binder and WC ceramics [54].

To summarize, cermet coatings' solid particle erosion mechanism relies on microcutting and grooving the metallic matrix, lip formation, detachment of carbides, and brittle cracking [50,55]. Compared to the samples deposited using a spray distance 320 mm, much severe deterioration has been observed for coatings sprayed from larger standoff (400 mm), resulting in lower hardness and uniformity obtained for cermet's sprayed with 400 mm. The longer spray distance influences the less compact structure and the reduced cohesion in the coating.

CONCLUSIONS

The main research goal of the current paper was to investigate the influence of spray distance and type of feedstock material on the erosion resistance of the WC-12Co, WC-10Co-4Cr and WC-20Cr₃C₂-7Ni cermet coatings deposited on magnesium alloy substrate by HVOF method. The successful manufacturing of the high-quality cermet coatings on the light AZ31 substrate was proved. Analysis of the results shows that spray distance is one of the key process parameters and influences the coating density, hardness and erosion resistance. On the other hand, the feedstock type negligibly influences these properties. The following findings can be summarized:

- the thickness of the deposited coatings was c.a. 250 μm and all the coatings have a dense and uniform structure. In addition, the irregularities of the substrate surface were well filled. Some defects such as cracks, pores and voids can be observed as a result of the HVOF thermal spray process;
- the porosity values of the manufactured coatings are at the level of typical HVOF deposits. Even for samples sprayed from 400 mm distance, the porosity is relatively low (up to 3 vol.%). Generally, coatings sprayed with a distance of 320 mm show lower porosity and higher hardness. C3-400 coating has the lowest hardness (912 HV0.2) and C1-320 has the highest hardness (1328 HV0.2). Reducing the spraying distance plays an important role in improving hardness. This is due to a denser structure and, consequently, lower porosity;
- the surface of the manufactured coating is relatively smooth for the coatings deposited, with a standoff distance equal to 320 mm. Minor irregularities can be observed in some places. At the spraying distance equal to 400 mm, some micro craters appeared, resulting in an increase in surface roughness. C3-400 coating has the highest roughness ($R_a = 4.60 \pm 0.34 \mu\text{m}$). The roughness decreases slightly with increasing spraying distance for coatings containing cobalt matrix. There was no clear relationship between the spray parameters, surface morphology of as-sprayed coatings, and erosion resistance;
- it can be clearly seen that the HVOF coating significantly improves the erosion resistance compared to the substrate material. The lowest average erosion rate (AER) is characterized by the C2-320 coating (0.54 mg/mm) with an impact angle of erodent equal to 30°, while the highest is the C3-400 coating (1.04 mg/mm) with an impact angle equal to 60°. Also, for average erosion value (AEV), the highest (approximately 0.0407 mm³/g) is characterized by the C3-400 coating with an impact angle of 60° and is the most hazardous for all cermet coatings. Dominant erosion mechanisms of cermet coatings were stated. Erosion relies on microcutting and grooving of the metallic matrix, material fatigue leading to brittle cracking, carbides and coating material removal;
- increasing each cermet hardness improves the erosion resistance. This depends on the microstructure and HVOF spray distance. A shorter

spray distance i.e. 320 mm decreases each coating's porosity and increases hardness, which both facilitate the erosion resistance of the coatings. In other words, all cermet coatings sprayed from 400 mm standoff distance show higher material loss than those deposited with 320 mm distance.

Acknowledgments

The authors would like to thank RESURS Company (Warsaw, Poland) for their help in the deposition of coatings.

REFERENCES

1. Alves H, Koster U, Aghion E, Eliezer D. Environmental behavior of magnesium and magnesium alloys. *materials technology*. 2001; 16: 110–26. <https://doi.org/10.1080/10667857.2001.11752920>.
2. Song G. Recent Progress in corrosion and protection of magnesium alloys. *Adv. Eng. Mater.* 2005; 7: 563–586. <https://doi.org/10.1002/adem.200500013>.
3. Liu B, Yang J, Zhang X, Yang Q, Zhang J, Li X. Development and application of magnesium alloy parts for automotive OEMs: A review. *Journal of Magnesium and Alloys*. 2023; 11: 15–47. <https://doi.org/10.1016/j.jma.2022.12.015>.
4. Tan J, Ramakrishna S. Applications of magnesium and its alloys: a review. *Applied Sciences*. 2021; 11: 6861. <https://doi.org/10.3390/app11156861>.
5. Kondaiah VV, Pavanteja P, Afzal Khan P, Anand Kumar S, Dumpala R, Ratna Sunil B. Microstructure, hardness and wear behavior of AZ31 Mg alloy – fly ash composites produced by friction stir processing. *Materials Today: Proceedings*. 2017; 4: 6671–6677. <https://doi.org/10.1016/j.matpr.2017.06.441>.
6. Song G-L, Xu Z. The surface, microstructure and corrosion of magnesium alloy AZ31 sheet. *Electrochimica Acta*. 2010; 55:4148–4161. <https://doi.org/10.1016/j.electacta.2010.02.068>.
7. Morelli S, Rombolà G, Bolelli G, Lopresti M, Puddu P, Bocaleri E, et al. Hard ultralight systems by thermal spray deposition of WC-CoCr onto AZ31 magnesium alloy. *Surface and Coatings Technology*. 2022; 451: 129056. <https://doi.org/10.1016/j.surfcoat.2022.129056>.
8. Oršulová T, Palček P. Changes in hardness of magnesium alloys due to precipitation hardening. *Production Engineering Archives*. 2018; 18: 46–9. <https://doi.org/10.30657/pea.2018.18.08>.
9. Akyuz B. A study on wear and machinability of AZ series (AZ01-AZ91) cast magnesium alloys. *Km*. 2016; 52: 255–62. https://doi.org/10.4149/km_2014_5_255.
10. Ishikawa Y, Kawakita J, Osawa S, Itsukaichi T, Sakamoto Y, Takaya M, et al. Evaluation of corrosion and wear resistance of hard cermet coatings sprayed by using an improved HVOF Process. *Journal of Thermal Spray Technology*. 2005; 14: 384–90. <https://doi.org/10.1361/105996305X59378>.
11. Ahmed R, Ali O, Berndt CC, Fardan A. Sliding wear of conventional and suspension sprayed nanocomposite WC-Co coatings: an invited review. *J Therm Spray Tech*. 2021; 30: 800–861. <https://doi.org/10.1007/s11666-021-01185-z>.
12. Singh J, Vasudev H, Szala M, Gill HS. Neural computing for erosion assessment in Al-20TiO₂ HVOF thermal spray coating. *Int. J. Interact. Des. Manuf.* 2023. <https://doi.org/10.1007/s12008-023-01372-y>.
13. Szala M, Walczak M, Łatka L, Gancarczyk K, Özkan D. Cavitation erosion and sliding wear of MCrAlY and NiCrMo Coatings Deposited by HVOF Thermal Spraying. *Advances in Materials Science*. 2020; 20: 26–38. <https://doi.org/10.2478/adms-2020-0008>.
14. Oksa M, Turunen E, Suhonen T, Varis T, Hannula S-P. Optimization and characterization of high velocity oxy-fuel sprayed coatings: techniques, materials, and applications. *Coatings*. 2011; 1:17–52. <https://doi.org/10.3390/coatings1010017>.
15. Ozimina D, Madej M, Kałdoński T. The Wear Resistance of HVOF sprayed composite coatings. *Tribol. Lett.* 2011; 41: 103–11. <https://doi.org/10.1007/s11249-010-9684-3>.
16. Goral M, Kubaszek T, Grabon WA, Grochalski K, Drajewicz M. The concept of WC-CrC-Ni plasma-sprayed coating with the addition of YSZ nanopowder for cylinder liner applications. *Materials*. 2023; 16: 1199. <https://doi.org/10.3390/ma16031199>.
17. Nowakowska M, Łatka L, Sokołowski P, Szala M, Toma F-L, Walczak M. Investigation into microstructure and mechanical properties effects on sliding wear and cavitation erosion of Al₂O₃-TiO₂ coatings sprayed by APS, SPS and S-HVOF. *Wear*. 2022; 508–509: 204462. <https://doi.org/10.1016/j.wear.2022.204462>.
18. Bolelli G, Lusvarghi L, Barletta M. HVOF-sprayed WC-CoCr coatings on al alloy: effect of the coating thickness on the tribological properties. *Wear*. 2009; 267: 944–953. <https://doi.org/10.1016/j.wear.2008.12.066>.
19. Puchi-Cabrera ES, Staia MH, Santana YY, Mora-Zorrilla EJ, Lesage J, Chicot D, et al. Fatigue behavior of AA7075-T6 aluminum alloy coated with a WC-10Co-4Cr cermet by HVOF thermal spray. *Surface and Coatings Technology*. 2013; 220: 122–30. <https://doi.org/10.1016/j.surfcoat.2012.04.087>.
20. Couto M, Dosta S, Guilemany JM. Comparison of

- the mechanical and electrochemical properties of WC-17 and 12Co coatings onto Al7075-T6 obtained by high velocity oxy-fuel and cold gas spraying. *Surface and Coatings Technology*. 2015; 268: 180–189. <https://doi.org/10.1016/j.surfcoat.2014.04.034>.
21. Varol Özkavak H, Şahin Ş, Saraç MF, Alkan Z. Comparison of wear properties of HVOF sprayed WC-Co and WC-CoCr coatings on Al alloys. *Mater. Res. Express*. 2019; 6: 096554. <https://doi.org/10.1088/2053-1591/ab2ee1>.
 22. Palanisamy K, Gangolu S, Mangalam Antony J. Effects of HVOF spray parameters on porosity and hardness of 316L SS coated Mg AZ80 alloy. *Surface and Coatings Technology*. 2022; 448:128898. <https://doi.org/10.1016/j.surfcoat.2022.128898>.
 23. Szala M, Walczak M, Świetlicki A. Effect of microstructure and hardness on cavitation erosion and dry sliding wear of HVOF deposited CoNiCrAlY, NiCoCrAlY and NiCrMoNbTa coatings. *Materials*. 2021; 15: 93. <https://doi.org/10.3390/ma15010093>.
 24. Jonda E, Łatka L, Godzierz M, Maciej A. Investigations of microstructure and corrosion resistance of WC-Co and WC-Cr₃C₂-Ni coatings deposited by HVOF on magnesium alloy substrates. *Surface and Coatings Technology*. 2023; 459: 129355. <https://doi.org/10.1016/j.surfcoat.2023.129355>.
 25. Fang W, Cho TY, Yoon JH, Song KO, Hur SK, Youn SJ. Processing optimization, surface properties and wear behavior of HVOF spraying WC–CrC–Ni coating. *Journal of Materials Processing Technology*. 2009; 209: 3561–3567. <https://doi.org/10.1016/j.jmatprotec.2008.08.024>.
 26. Jonda E, Szala M, Sroka M, Łatka L, Walczak M. Investigations of cavitation erosion and wear resistance of cermet coatings manufactured by HVOF spraying. *Applied Surface Science*. 2023; 608:155071. <https://doi.org/10.1016/j.apsusc.2022.155071>.
 27. Jonda E, Łatka L, Maciej A, Khozhanov A. Investigations on the microstructure and corrosion performance of different wc-based cermet coatings deposited by high velocity oxy fuel process onto magnesium alloy substrate. *Adv. Sci. Technol. Res. J*. 2023; 17: 25–35. <https://doi.org/10.12913/22998624/160513>.
 28. Jonda E, Łatka L, Tomiczek A, Godzierz M, Pakieła W, Nuckowski P. Microstructure investigation of wc-based coatings prepared by HVOF onto AZ31 substrate. *Materials*. 2021; 15: 40. <https://doi.org/10.3390/ma15010040>.
 29. Hong S, Wu Y, Wu J, Zhang Y, Zheng Y, Li J, et al. Microstructure and cavitation erosion behavior of HVOF sprayed ceramic-metal composite coatings for application in hydro-turbines. *Renewable Energy*. 2021; 164: 1089–1099. <https://doi.org/10.1016/j.renene.2020.08.099>.
 30. Wang H, Qiu Q, Gee M, Hou C, Liu X, Song X. Wear resistance enhancement of HVOF-sprayed WC-Co coating by complete densification of starting powder. *Materials & Design*. 2020; 191: 108586. <https://doi.org/10.1016/j.matdes.2020.108586>.
 31. Zhang H, Chen X, Gong Y, Tian Y, McDonald A, Li H. In-situ SEM observations of ultrasonic cavitation erosion behavior of HVOF-sprayed coatings. *Ultrasonics Sonochemistry*. 2020; 60: 104760. <https://doi.org/10.1016/j.ultsonch.2019.104760>.
 32. Yao H-L, Yang C, Yi D-L, Zhang M-X, Wang H-T, Chen Q-Y, et al. Microstructure and mechanical property of high velocity oxy-fuel sprayed WC-Cr₃C₂-Ni coatings. *Surface and Coatings Technology*. 2020; 397: 126010. <https://doi.org/10.1016/j.surfcoat.2020.126010>.
 33. Praveen AS, Arjunan A. High-temperature oxidation and erosion of HVOF sprayed NiCrSiB/Al₂O₃ and NiCrSiB/WC Co coatings. *Applied Surface Science Advances*. 2022; 7: 100191. <https://doi.org/10.1016/j.apsadv.2021.100191>.
 34. Sidhu HS, Sidhu BS, Prakash S. Mechanical and microstructural properties of HVOF sprayed WC–Co and Cr₃C₂–NiCr coatings on the boiler tube steels using LPG as the fuel gas. *Journal of Materials Processing Technology*. 2006; 171:77–82. <https://doi.org/10.1016/j.jmatprotec.2005.06.058>.
 35. Mishra TK, Kumar A, Sinha SK. Experimental investigation and study of HVOF sprayed WC-12Co, WC-10Co-4Cr and Cr₃C₂-25NiCr coating on its sliding wear behaviour. *International Journal of Refractory Metals and Hard Materials*. 2021; 94: 105404. <https://doi.org/10.1016/j.ijrmhm.2020.105404>.
 36. Yao H-L, Zhang M-X, Yang C, Chen Q-Y, Wang H-T, Bai X-B, et al. Microstructure and mechanical property of high velocity oxy-fuel sprayed multimodal WC-Cr₃C₂-Co-Y₂O₃ cermet coating. *Ceramics International*. 2020; 46:19431–19442. <https://doi.org/10.1016/j.ceramint.2020.04.288>.
 37. Testa V, Morelli S, Bolelli G, Benedetti B, Puddu P, Sassatelli P, et al. Alternative metallic matrices for WC-based HVOF coatings. *Surface and Coatings Technology*. 2020; 402: 126308. <https://doi.org/10.1016/j.surfcoat.2020.126308>.
 38. Raza A, Ahmad F, Badri TM, Raza MR, Malik K. An influence of oxygen flow rate and spray distance on the porosity of HVOF coating and its effects on corrosion—a review. *Materials*. 2022; 15:6329. <https://doi.org/10.3390/ma15186329>.
 39. Murugan K, Ragupathy A, Balasubramanian V, Sridhar K. Optimizing HVOF spray process parameters to attain minimum porosity and maximum hardness in WC–10Co–4Cr coatings. *Surface and Coatings Technology*. 2014; 247: 90–102. <https://doi.org/10.1016/j.surfcoat.2014.03.022>.
 40. Houdková Š, Bláhová O, Zahálka F, Kašparová M. The instrumented indentation study of

- HVOF-sprayed hardmetal coatings. *J Therm Spray Tech.* 2012; 21: 77–85. <https://doi.org/10.1007/s11666-011-9677-2>.
41. Goyal AK, Sapate SG, Mehar S, Vashishtha N, Bagde P, Rathod A. Tribological properties of HVOF sprayed WC-Cr₃C₂-Ni coating. *Mater Res Express.* 2019; 6: 106415. <https://doi.org/10.1088/2053-1591/ab3946>.
 42. Bolelli G, Berger L-M, Bonetti M, Lusvardi L. Comparative study of the dry sliding wear behaviour of HVOF-sprayed WC-(W,Cr)2C-Ni and WC-CoCr hardmetal coatings. *Wear.* 2014; 309:96–111. <https://doi.org/10.1016/j.wear.2013.11.001>.
 43. Yuan J, Ma C, Yang S, Yu Z, Li H. Improving the wear resistance of HVOF sprayed WC-Co coatings by adding submicron-sized WC particles at the splats' interfaces. *Surface and Coatings Technology.* 2016; 285: 17–23. <https://doi.org/10.1016/j.surfcoat.2015.11.017>.
 44. Agüero A, Camón F, García de Blas J, del Hoyo JC, Muelas R, Santaballa A, et al. HVOF-deposited WCCoCr as replacement for hard cr in landing gear actuators. *J Therm Spray Tech.* 2011; 20: 1292–309. <https://doi.org/10.1007/s11666-011-9686-1>.
 45. Komarov P, Jech D, Tkachenko S, Slámečka K, Dvořák K, Čelko L. Wetting behavior of wear-resistant WC-Co-Cr cermet coatings produced by HVOF: The role of chemical composition and surface roughness. *J Therm Spray Tech.* 2021; 30: 285–303. <https://doi.org/10.1007/s11666-020-01130-6>.
 46. Ding X, Ke D, Yuan C, Ding Z, Cheng X. Microstructure and cavitation erosion resistance of HVOF deposited WC-Co coatings with different sized WC. *Coatings.* 2018; 8: 307. <https://doi.org/10.3390/coatings8090307>.
 47. Karaoglanli AC, Oge M, Doleker KM, Hotamis M. Comparison of tribological properties of HVOF sprayed coatings with different composition. *Surface and Coatings Technology* 2017; 318: 299–308. <https://doi.org/10.1016/j.surfcoat.2017.02.021>.
 48. Cabral-Miramontes JA, Gaona-Tiburcio C, Almeraya-Calderón F, Estupiñan-Lopez FH, Pedraza-Basulto GK, Poblano-Salas CA. Parameter studies on high-velocity oxy-fuel spraying of CoNi-CrAlY coatings used in the aeronautical industry. *International Journal of Corrosion* 2014; 2014:1–8. <https://doi.org/10.1155/2014/703806>.
 49. Li Z, Li Y, Li J, Li F, Lu H, Du J, et al. Effect of NiCr content on the solid particle erosion behavior of NiCr-Cr3C2 coatings deposited by atmospheric plasma spraying. *Surface and Coatings Technology.* 2020; 381: 125144. <https://doi.org/10.1016/j.surfcoat.2019.125144>.
 50. González MA, Rodríguez E, Mojardín E, Jiménez O, Guillen H, Ibarra J. Study of the erosive wear behaviour of cryogenically and tempered WC-CoCr coating deposited by HVOF. *Wear.* 2017; 376–377: 595–607. <https://doi.org/10.1016/j.wear.2016.12.061>.
 51. Murthy JKN, Rao DS, Venkataraman B. Effect of grinding on the erosion behaviour of a WC-Co-Cr coating deposited by HVOF and detonation gun spray processes. *Wear* 2001; 249:592–600. [https://doi.org/10.1016/S0043-1648\(01\)00682-2](https://doi.org/10.1016/S0043-1648(01)00682-2).
 52. Thakur L, Arora N. A comparative study on slurry and dry erosion behaviour of HVOF sprayed WC-CoCr coatings. *Wear* 2013; 303:405–11. <https://doi.org/10.1016/j.wear.2013.03.028>.
 53. Zhang X, Li F, Li Y, Lu Q, Li Z, Lu H, et al. Comparison on multi-angle erosion behavior and mechanism of Cr3C2-NiCr coatings sprayed by SPS and HVOF. *Surface and Coatings Technology* 2020;403:126366. <https://doi.org/10.1016/j.surfcoat.2020.126366>.
 54. I. Hussainova. Some aspects of solid particle erosion of cermets. *Tribology International* 2001; 34:89–93. [https://doi.org/10.1016/S0301-679X\(00\)00140-7](https://doi.org/10.1016/S0301-679X(00)00140-7).
 55. Hutchings IM. Ductile-brittle transitions and wear maps for the erosion and abrasion of brittle materials. *J Phys D: Appl Phys* 1992;25:A212–21. <https://doi.org/10.1088/0022-3727/25/1A/033>.